Journal of Colloid and Interface Science 405 (2013) 278–290

Contents lists available at SciVerse ScienceDirect

Journal of Colloid and Interface Science

www.elsevier.com/locate/jcis

Forces acting on dielectric colloidal spheres at a water/nonpolar-fluid interface in an external electric field. 1. Uncharged particles

Krassimir D. Danov, Peter A. Kralchevsky *

Department of Chemical Engineering, Faculty of Chemistry and Pharmacy, Sofia University, 1164 Sofia, Bulgaria

ARTICLE INFO

Article history:
Received 18 March 2013
Accepted 7 May 2013
Available online 23 May 2013

Keywords:
Particles at a liquid interface
Non-densely packed interfacial colloid crystals
Particle arrays in external electric field
Contact angle
Electrodipping force
Mehler–Fock integral transform

ABSTRACT

Here, we calculate the electric forces acting on uncharged dielectric colloidal particles, which are attached to the interface between a nonpolar fluid (air, oil) and water, in the presence of an applied uniform external electric field directed normal to the interface. The uncharged particle becomes a source of dipolar electric field because it is polarized by the external field. Our goal is to calculate the normal (electrodipping) force acting on each separate particle, and the force of interaction between two identical particles. An exact analytical solution is obtained by solving the Laplace equation in toroidal coordinates and by separating the variables using the Mehler–Fock integral transform. The results show that the dependence of the normal force on particle contact angle is non-monotonic, with a maximum and a minimum. This force can be directed upward or downward depending on the particle contact angle and dielectric constant. An analytical asymptotic expression is derived for the force of interaction between two floating particles in external field. The magnitude of the latter force depends strongly on the particle contact angle α. At a certain value of α, the leading dipolar term becomes zero, and the interaction force is determined by the short-range octupolar term. Then, the attractive lateral capillary forces and van der Waals forces can overcome the electrostatic repulsion and can induce two-dimensional coagulation of the particles at the interface. The effects of the external electric field could find applications for control of the distances between particles in non-densely packed interfacial colloid crystals used in lithographic masks for the production of antireflective coatings, microlens arrays, etc. The case of charged particles in external field is considered in the second part of this study.

1. Introduction

In a previous paper [1], we solved analytically the electrostatic boundary problem for the field created by a spherical dielectric particle located at the interface between water and a nonpolar fluid (air, oil). It was assumed that the electric field is due to charges of surface density σ_{pn} located at the boundary particle-nonpolar fluid. Furthermore, the normal (electrodipping) force, $F^{(n)}$, acting on the particle was calculated at different values of the particle contact angle and dielectric constant. The calculation of $F^{(n)}$ is non-trivial, because the electric field has an integrable singularity at the particle three-phase contact line. This singularity gives a finite contribution to $F^{(n)}$. The problem was solved exactly by using toroidal coordinates and the Mehler–Fock integral transform. The results were also applied to calculate the force F_{12} of electrostatic repulsion between two floating charged particles [1].

Having determined the electric field near the water-nonpolar fluid interface, we calculated the interfacial shape (the shape of the capillary meniscus) around the particle. The theoretical results are in excellent agreement with the experimentally determined meniscus shape [2]. Knowing the meniscus shape, the next step was to calculate the electric-field-induced lateral capillary force between two particles at the interface and to compare this force (supposedly attractive) with the force of direct electrostatic repulsion between the particles. Both these forces are engendered by the electric charges on the particle surface. The results, which are valid in the asymptotic region of not-too-small interparticle distances, imply that the direct electrostatic repulsion always prevails over the electrocapillary attraction if the particle surface charges are uniformly distributed, i.e., σ_{pn} = const. [3]. This result is in agreement with the conclusions of other authors [4–6].

In the case of non-uniform distribution of the surface charges, their electric field induces a non-isotropic shape of the meniscus around the particle, the leading term being the quadrupolar one [7]. In the case of "heavy" particles that produce a concave meniscus due to their weight, the electric-field-induced quadrupolar meniscus of a given charged particles interacts with the isotropic gravitational concavity of the other particle. The latter interaction gives rise to a long-range hybrid capillary attraction that prevails over the direct electrostatic repulsion between two similar

* Corresponding author. Fax: +359 2 9625643.
E-mail address: pk@lcpe.uni-sofia.bg (P.A. Kralchevsky).

0021-9797/$ - see front matter © 2013 Elsevier Inc. All rights reserved.
http://dx.doi.org/10.1016/j.jcis.2013.05.020

particles and accelerates the particle motion toward each other on the liquid interface [8]. Another source of interparticle attraction can be the capillary force due to out-of-plane undulations of the contact line because of surface roughness or non-spherical particle shape [9–13], the so-called interactions between capillary multipoles [14–16].

Another way to induce electrostatic and electrocapillary interactions between particles attached to an interface is to apply an external electric field normal to the interface [17–22]. By varying the strength of the electric field, it is possible to control the distances between the particles in non-densely packed two-dimensional colloid crystals formed at liquid interfaces [17–20].

Non-densely packed particulate layers have been obtained by spreading of charged colloidal spheres on a liquid interface [23–30]. Such layers have found applications for the creation of lithographic masks for production of periodic nanostructures, e.g., antireflection coatings, microlens arrays, etc. [30–33]. The antireflection coatings from adsorbed colloid particles were inspired by the nanostructured corneas of moth eye, which consist of non-close-packed arrays of conical nipples [34]. As the periodicity of the nipple array is small compared to the wavelength of visible light, a gradual transition of the refractive index between air and cornea is established, which exhibits a superior broadband antireflection performance [33]. Another example are the structures of micro-lenses, which are widely used in many optical devices for increasing the brightness and homogeneity of color displays produced on the basis of light emitting diodes [35–37].

In the present article, we extend our approach from Ref. [1] to solve the problem for the forces acting on particles attached to a water-nonpolar fluid interface in the presence of a uniform external electric field, which is directed normal to the interface. In contrast to Ref. [1], here it is assumed that the dielectric particle is *uncharged* ($\sigma_{pn} = 0$), but it becomes a source of electric field because it is polarized by the external field. As in Ref. [1], the problem is solved by using the Mehler–Fock integral transform (Section 3), which allows the separation of the variables in boundary problems of similar geometry [38–40]. To simplify the problem, we consider particles of radius R, which is much greater than the Debye screening length in the water phase, i.e., $\kappa R \gg 1$. In such a case, the electrostatic interactions across the water phase are negligible and only the electric effects in the nonpolar fluid and inside the dielectric particle are essential [1]. For smaller particles ($\kappa R \leqslant 1$), the electrostatic effects in the aqueous phase can become significant [41–44]. The general solution of the problem is obtained by solving numerically an integral equation (Section 5). The numerical solution is tested against the analytical solution, which can be obtained in the special case of equal dielectric constants of the particle and the nonpolar fluid (Section 4). Furthermore, we calculate the normal (electrodipping) force $F^{(n)}$ acting on a single particle (Section 6), and the electrostatic interaction force F_{12} between two particles separated at not-too-short distances (Section 7). Special attention is paid to accurately estimate the contribution of the singularity of the electric field at the particle contact line (Sections 5.2 and 6.1 and Appendix A). The effects of particle contact angle α and dielectric constant ε_p on $F^{(n)}$ and F_{12} are investigated. For reader's convenience, the respective force coefficients are tabulated as functions of α and ε_p in Appendix B. Thus, the reader could simply calculate the normal and lateral forces, $F^{(n)}$ and F_{12}, acting on the particle by using a four-point interpolation formula, instead of repeating the time-consuming numerical solution of an integral equation (see below).

In part 2 of the present study, Ref. [45], the solution obtained in the present article is combined with that in Ref. [1] to calculate the forces acting on a *charged* particle ($\sigma_{pn} \neq 0$) in external field directed normal to the interface.

2. Physical system and theoretical approach

2.1. Formulation of the boundary problem

Let us consider an uncharged spherical particle of radius R, which is attached to the interface between water and a nonpolar fluid (air, oil, etc.), see Fig. 1. In zero-order approximation, we assume that the water-nonpolar fluid interface is planar. A uniform external electric field is applied perpendicular to the fluid interface, with a vertical projection E_0. The particle position is defined by the central angle, α, which coincides with the three-phase contact angle if the fluid interface is planar (Fig. 1). In accordance with the standard convention, $\alpha < 90°$ for a hydrophilic particle and $\alpha > 90°$ for a hydrophobic particle. The three-phase contact line is a circumference of radius r_c.

The applied external electric field causes polarization of the dielectric particle, so that the total electric field near the particle is non-uniform. As already mentioned, our goal is to describe theoretically this field, to calculate the electrodipping force acting on the particle, as well as the force of electrostatic interaction between two such particles in the external field. The potential of the electric field, φ_p inside the particle and φ_n in the nonpolar fluid, obeys the Laplace equation,

$$\nabla^2\varphi_p = 0 \quad \text{in} \quad \Omega_p \quad \text{and} \quad \nabla^2\varphi_n = 0 \quad \text{in} \quad \Omega_n, \tag{2.1}$$

where ∇^2 is the Laplace operator, Ω_p and Ω_n are the spatial domains occupied by the particle and nonpolar fluid, respectively.

Let us denote the dielectric constants of the water, nonpolar fluid and particle ε_w, ε_n and ε_p, respectively. As in Ref. [1], we assume that $\varepsilon_w \gg \varepsilon_p, \varepsilon_n$. For this reason, the electric field in the nonpolar phases Ω_p and Ω_n practically does not penetrate into the water phase; see, for example, the conventional problem for the image force [46] and for a charged hydrophobic particle near the oil–water interface [47]. Experimentally, the non-penetration of the field into water is manifested as independence of the configuration of the adsorbed particles on the electrolyte concentration in the aqueous phase [25,48].

Thus, in first approximation, the role of the water is to keep the electric potential constant at the boundaries S_{nw} and S_{pw} (Fig. 1). Because the latter constant can be set zero, we obtain the following two boundary conditions:

$$\varphi_p = 0 \quad \text{at} \quad S_{pw} \quad \text{and} \quad \varphi_n = 0 \quad \text{at} \quad S_{nw}. \tag{2.2}$$

At S_{pn}, we impose the standard boundary conditions for continuity of the electric potential and the relation between the normal electric-field components in the absence of charges on the particle surface:

$$\varphi_n = \varphi_p \quad \text{and} \quad \mathbf{n}\cdot(\varepsilon_p\nabla\varphi_p - \varepsilon_n\nabla\varphi_n) = 0 \quad \text{at} \quad S_{pn}, \tag{2.3}$$

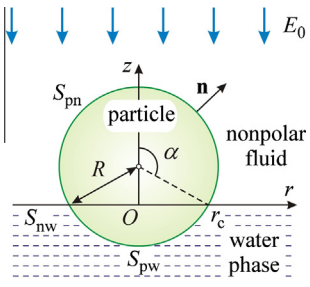

Fig. 1. Sketch of an uncharged colloidal sphere attached to the water–nonpolar fluid interface, S_{nw}. The particle–nonpolar fluid and particle–water interfaces are denoted S_{pn} and S_{pw}, respectively; $\mathbf{n}$ is the outer unit normal to S_{pn}; E_0 is a uniform external field.

where ∇ is the del operator and $\mathbf{n}$ is the outer unit normal to S_{pn} (Fig. 1). In the nonpolar fluid at large distances from the particle, the external electric field is $\mathbf{E}_0 = -E_0\mathbf{e}_z$, where $\mathbf{e}_z$ is the unit vector of the vertical axis z (Fig. 1). Then, the electric potential should have the following asymptotic form:

$$\varphi_n \to E_0 z \quad \text{far from the particle.} \tag{2.4}$$

2.2. Toroidal coordinates

As in Ref. [1], we introduce the conventional toroidal coordinates, ξ and η, defined as follows [49]:

$$r = \frac{r_c}{h}\sinh\eta \quad \text{and} \quad z = \frac{r_c}{h}\sin\xi, \tag{2.5}$$

where h is a metric coefficient:

$$h = \cosh\eta - \cos\xi. \tag{2.6}$$

The Lamé coefficients of the toroidal coordinate system are [49]:

$$h_\xi = h_\eta = \frac{r_c}{h} \quad \text{and} \quad h_\phi = \frac{r_c}{h}\sinh\eta. \tag{2.7}$$

The position of the contact line is determined by the pole, A_+ ($\eta \to +\infty$) (see Fig. 2). The axis of revolution corresponds to $\eta = 0$; the interfaces S_{nw}, S_{pn}, and S_{pw} have equations $\xi = 0$, $\xi = \xi_c$, and $\xi = \pi + \xi_c$, respectively, where

$$\xi_c = \pi - \alpha. \tag{2.8}$$

The electrostatic potentials in the nonpolar fluid and in the particle, φ_n and φ_p, can be expressed in terms of respective dimensionless potentials, Φ_n and Φ_p, as follows:

$$\varphi_n \equiv E_0 r_c\left(\frac{z}{r_c} + \Phi_n\right) \quad \text{and} \quad \varphi_p \equiv E_0 r_c\left(\frac{z}{r_c} + \Phi_p\right). \tag{2.9}$$

The term z/r_c in the parentheses is introduced in view of Eq. (2.4). Because of the axial symmetry of the system, in toroidal coordinates Eq. (2.1) acquires the form [1]

$$\frac{\partial}{\partial\xi}\left(\frac{\sinh\eta}{h}\frac{\partial\Phi_k}{\partial\xi}\right) + \frac{\partial}{\partial\eta}\left(\frac{\sinh\eta}{h}\frac{\partial\Phi_k}{\partial\eta}\right) = 0 \quad \text{in} \quad \Omega_k \ (k = \text{n, p}). \tag{2.10}$$

Correspondingly, the boundary conditions, Eqs. (2.2)–(2.4), become

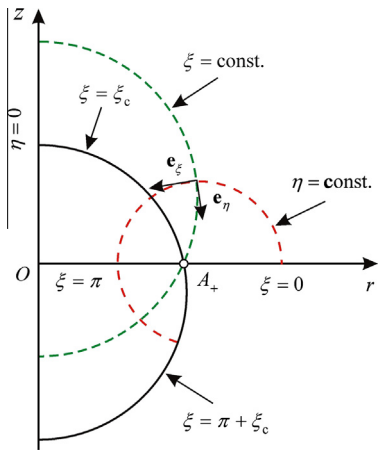

Fig. 2. Toroidal coordinates (ξ, η): The particle surface, shown with a solid line, consists of S_{pn} and S_{pw} (Fig. 1), which correspond to the coordinate surfaces $\xi = \xi_c$ and $\xi = \pi + \xi_c = 2\pi - \alpha$, respectively. The interface S_{nw} corresponds to the coordinate surface $\xi = 0$. The position of the contact line coincides with the pole A_+.

$$\Phi_n = 0 \quad \text{at} \quad \xi = 0 \quad \text{and} \quad \Phi_p = -\frac{z}{r_c} \quad \text{at} \quad \xi = \pi + \xi_c, \tag{2.11}$$

$$\Phi_n = \Phi_p \quad \text{and} \quad \varepsilon_p\frac{\partial\Phi_p}{\partial\xi} - \varepsilon_n\frac{\partial\Phi_n}{\partial\xi} = (\varepsilon_n - \varepsilon_p)\frac{\partial}{\partial\xi}\left(\frac{z}{r_c}\right) \text{ at } \xi = \xi_c, \tag{2.12}$$

$$\Phi_n \to 0 \quad \text{far from the particle.} \tag{2.13}$$

At S_{nw}, the tangential component of the electric field in the nonpolar fluid is zero and the normal components is

$$E_z = -E_0 - E_0(\cosh\eta - 1)\frac{\partial\Phi_n}{\partial\xi} \quad \text{at} \quad \xi = 0. \tag{2.14}$$

Our next goal is to determine $E_z(\eta)$ at $\xi = 0$, because both the electrodipping force and the asymptotics of the electric force between two particles are expressed as integrals of this function; see below.

3. Solution by the Mehler–Fock integral transform

3.1. Basic equations

To separate variables in Eq. (2.10), the following substitution can be used [1,50–52]:

$$\Phi_k \equiv h^{1/2}\Psi_k \quad (k = \text{n, p}). \tag{3.1}$$

Next, Ψ_k can be expressed using the Mehler–Fock transform [1,52–58]:

$$\Psi_k(\xi,\eta) = \int_0^\infty B_k(\xi,\tau)K(\eta,\tau)d\tau \quad (k = \text{n, p}), \tag{3.2}$$

where $B_k(\xi,\tau)$ is the respective Mehler–Fock image. By definition, the kernel is

$$K(\eta,\tau) \equiv P_{-1/2+i\tau}(\cosh\eta), \tag{3.3}$$

where i is the imaginary unit, $P_{-1/2+i\tau}$ is the Legendre function of the first kind and complex index $-1/2 + i\tau$. The substitution of Eqs. (3.1) and (3.2) into Eq. (2.10) yields [1]

$$\frac{\partial^2 B_k}{\partial\xi^2} = \tau^2 B_k \quad \text{in} \quad \Omega_k \quad (k = \text{n, p}). \tag{3.4}$$

The solution of the latter equations is:

$$B_n(\xi,\tau) = \Psi_b(\tau)\frac{\sinh(\xi\tau)}{\sinh(\xi_c\tau)}, \tag{3.5}$$

$$B_p(\xi,\tau) = \Psi_b(\tau)\frac{\sinh[(\pi + \xi_c - \xi)\tau]}{\sinh(\pi\tau)} + \Psi_w(\tau)\frac{\sinh[(\xi - \xi_c)\tau]}{\sinh(\pi\tau)}. \tag{3.6}$$

$\Psi_b(\tau)$ is the image of the dimensionless electric potential at the particle–nonpolar fluid boundary, S_{pn}; $\Psi_w(\tau)$ is the respective image at the particle–water boundary, S_{pw}. Eqs. (3.5) and (3.6) satisfy the boundary conditions $\Phi_n = 0$ at $\xi = 0$ and $\Phi_n = \Phi_p$ at $\xi = \xi_c$; see Eqs. (2.11) and (2.12).

Using Eqs. (2.5), (2.6), and (3.1), we bring the second boundary condition in Eq. (2.11) in the form:

$$\Psi_p\big|_{\xi=\pi+\xi_c} = -\frac{\sin(\pi + \xi_c)}{[\cosh\eta - \cos(\pi + \xi_c)]^{3/2}}. \tag{3.7}$$

The right-hand side of Eq. (3.7) can be transformed by means of the formula [1,59]:

$$\frac{\sin u}{(\cosh\eta - \cos u)^{3/2}} = 2^{3/2}\int_0^\infty \tau\frac{\sinh[(\pi - u)\tau]}{\cosh(\pi\tau)}K(\eta,\tau)d\tau \quad \text{for} \quad 0 < u < 2\pi. \tag{3.8}$$

Combining Eqs. (3.2), (3.3), (3.6), (3.7), and (3.8), we obtain an explicit expression for $\Psi_w(\tau)$:

$$\Psi_w(\tau) = 2^{3/2}\tau\frac{\sinh(\xi_c\tau)}{\cosh(\pi\tau)}. \tag{3.9}$$

Furthermore, to determine $\Psi_b(\tau)$ we have to use the second boundary condition in Eq. (2.12). As shown in Appendix A, it can be represented in the form of an integral equation for $\Psi_b(\tau)$:

$$\int_0^\infty \left\{[\coth(\xi_c\tau) + \varepsilon_{pn}\coth(\pi\tau)]\Psi_b - \frac{2^{3/2}W(\tau)}{\cosh(\pi\tau)}\right\}\tau K(\eta,\tau)d\tau = -\frac{(1-\varepsilon_{pn})\sin\xi_c}{2(\cosh\eta - \cos\xi_c)}\int_0^\infty \Psi_b K(\eta,\tau)d\tau, \tag{3.10}$$

where $\varepsilon_{pn} = \varepsilon_p/\varepsilon_n$ and

$$W(\tau) = \frac{\varepsilon_{pn}\tau\sinh(\xi_c\tau)}{\sinh(\pi\tau)} + \frac{1-\varepsilon_{pn}}{3}\{2\tau\cosh[(\pi-\xi_c)\tau] - \cot\xi_c\sinh[(\pi-\xi_c)\tau]\}. \tag{3.11}$$

Eq. (3.10) represents a Fredholm integral equation of the second kind, which has a convenient numerical solution for $\Psi_b(\tau)$. The respective numerical procedure is much faster than the procedure for direct solving the partial differential equations [1]. In addition, Eq. (3.11) will be used to derive useful asymptotic expressions for the behavior of the physical variables near the contact line and far from it. For $\varepsilon_{pn} = 1$, Eq. (3.10) has an explicit analytical solution for $\Psi_b(\tau)$, which is described in Section 4.

3.2. The electric field at the water–nonpolar fluid interface

At S_{nw}, the tangential component of the electric field in the nonpolar fluid is equal to zero because $\Phi_n = 0$ at $\xi = 0$; see Eq. (2.11). At S_{nw}, the normal component E_z can be calculated from the expression

$$E_z = -E_0 - E_0(\cosh\eta - 1)^{3/2}I_E(\eta,\alpha,\varepsilon_{pn}),$$

$$I_E(\eta,\alpha,\varepsilon_{pn}) \equiv \int_0^\infty \frac{\tau\Psi_b(\tau)}{\sinh(\xi_c\tau)}K(\eta,\tau)d\tau, \tag{3.12}$$

which follows from Eqs. (2.14), (3.1), (3.2), and (3.5). The planar interface S_{nw} corresponds to the domain $r_c < r < \infty$ or, respectively, $\infty > \tau > 0$. It is convenient to introduce the new variable, x_1, which has a finite domain of variation [1]:

$$x_1 \equiv \frac{r_c}{r} = \frac{\cosh\eta - 1}{\sinh\eta} \quad (0 < x_1 < 1). \tag{3.13}$$

Eq. (3.13) can be represented also in the form:

$$\cosh\eta - 1 = \frac{2x_1^2}{1-x_1^2} \quad \text{and} \quad \exp\eta = \frac{1+x_1}{1-x_1}. \tag{3.14}$$

The substitution of Eq. (3.14) into Eq. (3.12) yields:

$$E_z = -E_0 - E_0\frac{2^{3/2}x_1^3}{(1-x_1^2)^{3/2}}\int_0^\infty \frac{\tau\Psi_b(\tau)}{\sinh(\xi_c\tau)}K(\eta,\tau)d\tau. \tag{3.15}$$

Using the asymptotic expansion of $K(\eta,\tau)$ for $\eta \to 0$ from Ref. [60], we derive:

$$\frac{x_1^3}{(1-x_1^2)^{3/2}}K(\eta,\tau) = x_1^3 + \left(\frac{5}{4} - \tau^2\right)x_1^5 + O(x_1^7). \tag{3.16}$$

Eqs. (3.15) and (3.16) lead to the following asymptotic expansion for the electric field:

$$E_z = -E_0 - E_0[H_3x_1^3 + H_5x_1^5 + O(x_1^7)]. \tag{3.17}$$

where the coefficients are:

$$H_3(\alpha,\varepsilon_{pn}) = 2^{3/2}\int_0^\infty \frac{\tau\Psi_b(\tau)}{\sinh(\xi_c\tau)}d\tau, \tag{3.18}$$

$$H_5(\alpha,\varepsilon_{pn}) = 2^{3/2}\int_0^\infty \frac{\tau\Psi_b(\tau)}{\sinh(\xi_c\tau)}\left(\frac{5}{4} - \tau^2\right)d\tau. \tag{3.19}$$

We recall that by definition $\xi_c = \pi - \alpha$.

E_z has a weak singularity at $x_1 \to 1$, at the three-phase contact line. To find an asymptotic expression for E_z in the vicinity of this singular point, we represent Eq. (3.15) in the form [1]:

$$E_z = -E_0 - E_0\frac{x_1^3 J_E}{(1-x_1)^{1-\nu}},$$

$$J_E(x_1,\alpha,\varepsilon_{pn}) \equiv \frac{2^{3/2}I_E(\eta,\alpha,\varepsilon_{pn})}{(1+x_1)^{3/2}(1-x_1)^{\nu+1/2}}. \tag{3.20}$$

where J_E is a function of bounded variation. The parameter ν depends on the central angle, α, and the dielectric constant ratio, $\varepsilon_{pn} = \varepsilon_p/\varepsilon_n$. Values of the function $\nu(\alpha, \varepsilon_{pn})$ are given in Table 1 of Appendix B. In general, $0.5 \leqslant \nu \leqslant 1$. For $x_1 \ll 1$ (near the contact line), Eq. (3.20) acquires the form:

$$E_z = -E_0 - E_0J_{E1}(1-x_1)^{\nu-1} \quad (x_1 \to 1), \tag{3.21}$$

where

$$J_{E1}(\alpha,\varepsilon_{pn}) \equiv J_E(1,\alpha,\varepsilon_{pn}) = \lim_{x_1\to 1}\left[\frac{I_E(\eta,\alpha,\varepsilon_{pn})}{(1-x_1)^{\nu+1/2}}\right]. \tag{3.22}$$

In Section 5.2, the values of $J_{E1}(\alpha,\varepsilon_{pn})$ are calculated and listed in Table 2 of Appendix B.

4. Solutions to the problem for $\varepsilon_p = \varepsilon_n$ and $\varepsilon_p \gg \varepsilon_n$

4.1. Analytical solution for $\varepsilon_p = \varepsilon_n$

Examples for particle and nonpolar liquid that have equal dielectric constants are (i) glass and isopropyl ether with $\varepsilon_p \approx \varepsilon_n \approx 3.9$ and (ii) polystyrol and hexadecane with $\varepsilon_p \approx \varepsilon_n \approx 2.0$. Many solid plastics and organic liquids have close dielectric constants.

For $\varepsilon_{pn} = 1$, Eq. (3.10), along with Eq. (3.11), has the following analytical solution:

$$\Psi_b(\tau) = \frac{2^{3/2}\tau\sinh^2(\xi_c\tau)}{\cosh(\pi\tau)\sinh[(\pi+\xi_c)\tau]} \tag{4.1}$$

($\xi_c = \pi - \alpha$). The substitution of Eq. (4.1) into Eqs. (3.18) and (3.19) gives $H_3(\alpha,1)$ and $H_5(\alpha,1)$ in the form of definite integrals that can be solved numerically. Fig. 3 shows $H_3(\alpha,1)$ and $H_5(\alpha,1)$ calculated

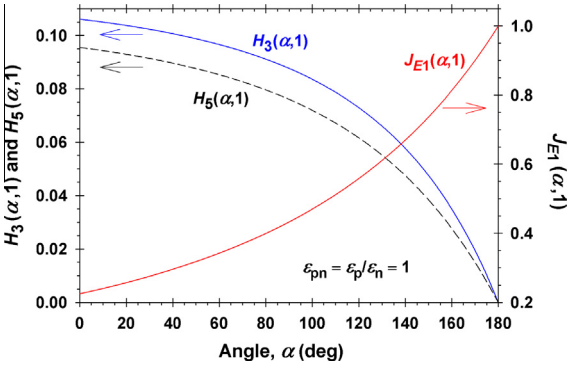

Fig. 3. Plots of $H_3(\alpha,1)$, $H_5(\alpha,1)$, and $J_{E1}(\alpha,1) \equiv J_E(1,\alpha,1)$ vs. the central angle α calculated by means of Eqs. (3.18), (3.19), (4.1), and (4.8).

in this way for $0 < \alpha < \pi$. The special values of these functions at the end points are:

$$H_3(\pi,1) = H_5(\pi,1) = 0, \tag{4.2}$$

$$H_3(0,1) = \frac{1}{3\pi} \quad \text{and} \quad H_5(0,1) = \frac{3}{10\pi}. \tag{4.3}$$

Eq. (4.2) means that at $\alpha = \pi$ the effect of particle on the electric field far from it is zero, see Eq. (3.17), as it should be, because at $\alpha = \pi$ the particle is completely immersed in the nonpolar fluid of the same dielectric constant ($\varepsilon_{pn} = 1$). The vertical displacement of the particle toward the water phase (the decrease in α) leads to increasing of both $H_3(\alpha,1)$ and $H_5(\alpha,1)$, and of the effect of particle on the electric field (Fig. 3). It is interesting that the latter effect becomes maximal for $\alpha = 0$, i.e., for a particle that is completely immersed in the water phase; see also Eq. (4.3).

Eq. (3.17), where H_3 and H_5 are coefficients functions, gives E_z for $x_1 \ll 1$, i.e., far from the particle. To find E_z in the whole interval $0 < x_1 < 1$, we have to calculate J_E in Eq. (6.1). To do that, we substitute Eq. (4.1) in Eq. (3.12) and use the relation between I_E and J_E in Eq. (3.20). After some mathematical transformations described in Appendix A, we arrive at the following expression for J_E in terms of a definite integral of elementary functions:

$$J_E(x_1,\alpha,1) = \frac{16\nu_e^2 \sin(\nu_e\pi)}{\pi(2\nu_e+1)} \int_0^{t_1} S_1(x_1,\alpha,t) S_2(x_1,\alpha,t)\,dt, \tag{4.4}$$

$$S_1 = \frac{1-(1-x_1)^2 t^{2\omega_e}}{[1+x_1+2(1+x_1^2)t^{\omega_e}+(1+x_1)(1-x_1)^2 t^{2\omega_e}]^{3/2}}, \tag{4.5}$$

$$S_2 = \frac{1-(1-x_1)^{2\nu_e} t^{2\nu_e\omega_e}}{[1-2\cos(\nu_e\pi)(1-x_1)^{\nu_e} t^{\nu_e\omega_e}+(1-x_1)^{2\nu_e} t^{2\nu_e\omega_e}]^2}, \tag{4.6}$$

$$\nu_e = \frac{\pi}{2\pi-\alpha} \quad \omega_e \equiv \frac{2}{2\nu_e+1}, \quad t_1 \equiv (1-x_1)^{-(\nu_e+1/2)}. \tag{4.7}$$

Here, by definition $\nu_e \equiv \nu(\alpha,1)$; see Table 1 in Appendix B. Dependences of J_E on x_1, calculated from Eqs. (4.4)–(4.7) at various α, are shown in Fig. 4. The variation of J_E with x_1 is weak far from the particle, but J_E steeply increases at $x_1 \to 1$, i.e., near the contact line on the particle surface (Fig. 4a). The variation of J_E at $x_1 \to 1$ is visualized in Fig. 4b. The limiting value of J_E at $x_1 = 1$ (at the contact line), $J_{E1}(\alpha,1)$, is plotted in Fig. 3 vs. α; see also Eq. (3.22). One sees that $J_{E1}(\alpha,1)$ monotonically increases with the rise of the contact angle α.

Explicit analytical expression for $J_{E1}(\alpha,1)$ can be obtained by setting $x_1 \to 1$ in Eqs. (4.4)–(4.7):

$$J_{E1}(\alpha,1) = \frac{16\nu_e^2 \sin(\nu_e\pi)}{\pi(2\nu_e+1)} \int_0^{\infty} \frac{dt}{(2+4t^{\omega_e})^{3/2}} = \frac{2^{2-\nu_e}\nu_e^2}{\pi^{1/2}} \frac{\Gamma(0.5+\nu_e)}{\Gamma(\nu_e)}, \tag{4.8}$$

where Γ is the known gamma function [49,60]. For $\alpha = 0$, we have $J_{E1}(0,1) = 1/(2^{1/2}\pi) \approx 0.225$; see also Fig. 3.

4.2. Analytical solution for $\varepsilon_p \gg \varepsilon_n$

For example, the dielectric constant ε_p of TiO_2 particles is 40 for anatase and 86–170 (depending on crystal orientation) for rutile [61–63]. At $\varepsilon_p \gg \varepsilon_n$, the electric potential in the particle phase is the same as in the water phase. Thus, the boundary condition, Eq. (2.3), reduces to

$$\varphi_n = 0 \quad \text{at} \quad S_{pn}. \tag{4.9}$$

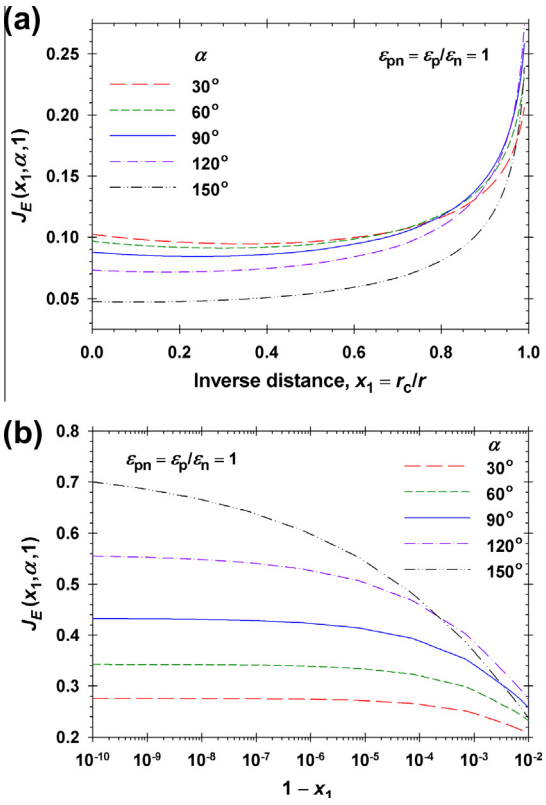

Fig. 4. Plots of $J_E(x_1,\alpha,1)$ vs. x_1 at different values of the central angle α: (a) for $0 \leqslant x_1 < 0.99$; (b) close to the three-phase contact line for $10^{-10} \leqslant 1 - x_1 \leqslant 10^{-2}$.

With the help of Eqs. (2.5), (2.6), (2.9), and (3.1), Eq. (4.9) acquires the form:

$$\Psi_n|_{\xi=\xi_c} = -\frac{\sin\xi_c}{(\cosh\eta - \cos\xi_c)^{3/2}}. \tag{4.10}$$

Further, combining Eqs. (3.5), (3.8), and (4.10) we obtain:

$$\Psi_b(\tau) = -2^{3/2}\tau \frac{\sinh[(\pi-\xi_c)\tau]}{\cosh(\pi\tau)}. \tag{4.11}$$

The comparison of Eqs. (4.1) and (4.11) shows that in the respective two limiting cases, Ψ_b (and the electric field due to the particle) has the opposite signs; see also Eq. (3.15). Hence, the electric field created by the particle *enhances* the external field $\mathbf{E}_0$ for $\varepsilon_p = \varepsilon_n$, but *opposes* the external field for $\varepsilon_p \gg \varepsilon_n$.

The substitution of Eq. (4.11) into Eqs. (3.18) and (3.19) gives $H_3(\alpha,1)$ and $H_5(\alpha,1)$ in the form of definite integrals that can be solved numerically. Some special values of these functions at the end points are:

$$H_3(0,\infty) = H_5(0,\infty) = 0, \tag{4.12}$$

$$H_3(\pi/2,\infty) = -1, \quad H_5(\pi/2,\infty) = 0, \tag{4.13}$$

$$H_3(\pi,\infty) = -\infty \quad \text{and} \quad H_5(\pi,\infty) = +\infty. \tag{4.14}$$

The divergence in Eq. (4.14) is related to the scaling of $x_1 = r_c/r$, and to the fact that $r_c \to 0$ for $\alpha \to \pi$; see also Eq. (3.17). It is convenient to rescale H_3 and H_5 using the parameter:

$$A = \frac{2\pi R^2(1-\cos\alpha)}{\pi r_c^2} = \frac{2}{1+\cos\alpha}. \tag{4.15}$$

A is equal to the area of S_{pn} divided by the area encircled by the contact line (Fig. 1). As seen in Fig. 5, the rescaled functions $H_3(\alpha,\infty)/$

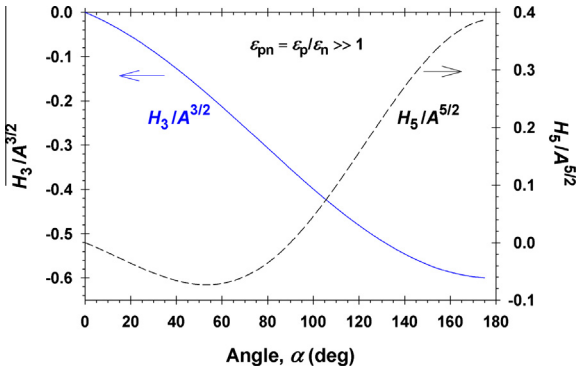

Fig. 5. Dependences of $H_3(\alpha,\infty)/A^{3/2}$ and $H_5(\alpha,\infty)/A^{5/2}$ on the central angle α.

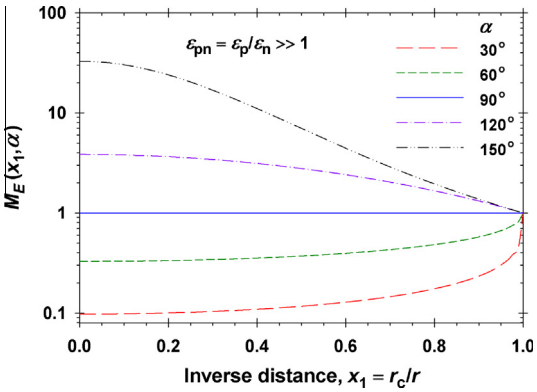

Fig. 6. Plots of M_E vs. x_1 calculated from Eqs. (4.17)–(4.19) at different α values.

$A^{3/2}$ and $H_5(\alpha,\infty)/A^{5/2}$ have bounded variation. H_3 is negative for all $0 < \alpha < \pi$, whereas H_5 is negative for hydrophilic particles ($\alpha < \pi/2$), and positive for hydrophobic ones ($\alpha > \pi/2$).

In the case $\varepsilon_p \gg \varepsilon_n$, the weak singularity of E_z at the contact line ($x_1 \to 1$) disappears. For this reason, it is convenient to represent Eq. (3.12) in the form:

$$E_{E,z} = -E_0 + E_0 x_1^3 M_E(x_1,\alpha),$$

$$M_E(x_1,\alpha) \equiv -\frac{2^{3/2}}{(1-x_1^2)^{3/2}} I_E(\eta,\alpha,\infty). \tag{4.16}$$

Substituting Eq. (4.11) under the integral in Eq. (3.12) and using Eq. (4.16), one can derive (see Appendix A):

$$M_E = \frac{32}{\pi}\int_0^1 \frac{S_3(x_1,\alpha,u)du}{[(1+x_1)^2+(1-x_1)^2u^4-2u^2(1+x_1^2)]^{1/2}}, \tag{4.17}$$

$$S_3 = \frac{[1+x_1+(1-x_1)u^2]}{[1+x_1-(1-x_1)u^2]^3}u^2 - \lambda_e^3(1-x_1^2)^{\lambda_e-1} \times \frac{[(1+x_1)^{\lambda_e}+(1-x_1)^{\lambda_e}u^{2\lambda_e}]}{[(1+x_1)^{\lambda_e}-(1-x_1)^{\lambda_e}u^{2\lambda_e}]^3}u^{2\lambda_e} \tag{4.18}$$

$$\lambda_e \equiv \frac{\pi}{\pi-\alpha} = \frac{\nu_e}{1-\nu_e}. \tag{4.19}$$

At the contact line, $x_1 = 1$, we have $S_3 = u^2/4$ and Eq. (4.17) reduces to

$$M_E(1,\alpha) = \frac{4}{\pi}\int_0^1 \frac{u^2du}{(1-u^2)^{1/2}} = 1 \tag{4.20}$$

for all $0 \leqslant \alpha \leqslant \pi$. Fig. 6 shows plots of M_E vs. x_1 calculated from Eqs. (4.17)–(4.19) at different values of the contact angle α. M_E is positive for hydrophilic particles ($\alpha < \pi/2$) and negative for hydrophobic particles ($\alpha > \pi/2$).

For $\alpha = 90°$, M_E is identically equal to 1 (Fig. 6). In this case, the electrostatic potential in the nonpolar fluid is described by the simple expression:

$$\varphi_n = E_0 z - E_0 z\frac{r_c^3}{(r^2+z^2)^{3/2}}. \tag{4.21}$$

Eq. (4.21) expresses φ_n as a superposition of the external field and the field of a dipole.

5. Solution to the general problem

5.1. Reduction of the problem to Fredholm equation

Following the approach from Ref. [1], in Appendix A, we have demonstrated that Eq. (3.10) can be represented as a Fredholm equation of the second kind:

$$G(\tau) = b(\tau) + \int_0^\infty V(\tau,\tilde\tau)G(\tilde\tau)d\tilde\tau, \tag{5.1}$$

where

$$V(\tau,\tilde\tau) \equiv \beta\sin(\alpha)g(\tau)g(\tilde\tau)U(\tau,\tilde\tau), \tag{5.2}$$

$$G(\tau) \equiv \frac{\Psi_b(\tau)}{g(\tau)}, \quad \beta \equiv \frac{\varepsilon_{pn}-1}{\varepsilon_{pn}+1}, \tag{5.3}$$

$$U(\tau,\tilde\tau) \equiv \int_0^\infty \frac{K(\eta,\tau)K(\eta,\tilde\tau)}{\cosh\eta+\cos\alpha}\sinh\eta d\eta. \tag{5.4}$$

$$g^2(\tau) \equiv \frac{\sinh(\pi\tau)\sinh[(\pi-\alpha)\tau]\tanh(\pi\tau)}{\sinh[(2\pi-\alpha)\tau]-\beta\sinh(\alpha\tau)}. \tag{5.5}$$

$$b(\tau) \equiv 2^{3/2}\left\{(1+\beta)\frac{\tau\sinh[(\pi-\alpha)\tau]}{\sinh^2(\pi\tau)} - \frac{2\beta}{3}\left[\cot\alpha\frac{\sinh(\alpha\tau)}{\sinh(\pi\tau)} + 2\tau\frac{\cosh(\alpha\tau)}{\sinh(\pi\tau)}\right]\right\}g(\tau). \tag{5.6}$$

The functions b^2 and V^2 are integrable over the domain $0 < \tau < \infty$. Moreover, $V(\tau,\tilde\tau)$ is a symmetric function of its arguments. In such a case, $G(\tau)$ can be found as a solution of Eq. (5.1) by iterations [64]. To start the iterations, we substitute $G(\tilde\tau) = b(\tilde\tau)$ in the right-hand side of Eq. (5.1). For fast calculation of the kernels K and U in Eq. (5.4), we used the procedure described in Appendix C of Ref. [1].

The function U defined by Eq. (5.4) depends on α, but it is independent of ε_{pn}. For this reason, we calculated U and stored the dependence of U on α. The stored numerical data were further used to compute the parameters listed in the tables in Appendix B at various ε_{pn}.

5.2. Numerical results

Having determined $\Psi_b(\tau)$ as explained in Section 5.1, by numerical integration in Eqs. (3.18) and (3.19), we calculated the coefficient functions $H_3(\alpha,\varepsilon_{pn})$ and $H_5(\alpha,\varepsilon_{pn})$ in the expansion, Eq. (3.17). The latter expansion gives the asymptotics of E_z far from the particle. Results for $H_3(\alpha,\varepsilon_{pn})$ and $H_5(\alpha,\varepsilon_{pn})$ are plotted in Fig. 7 and tabulated in Tables 3 and 4 of Appendix B. In particular, Fig. 7 shows the plots of $H_3/A^{3/2}$ and $H_5/A^{5/2}$ vs. α at various ε_{pn} values.

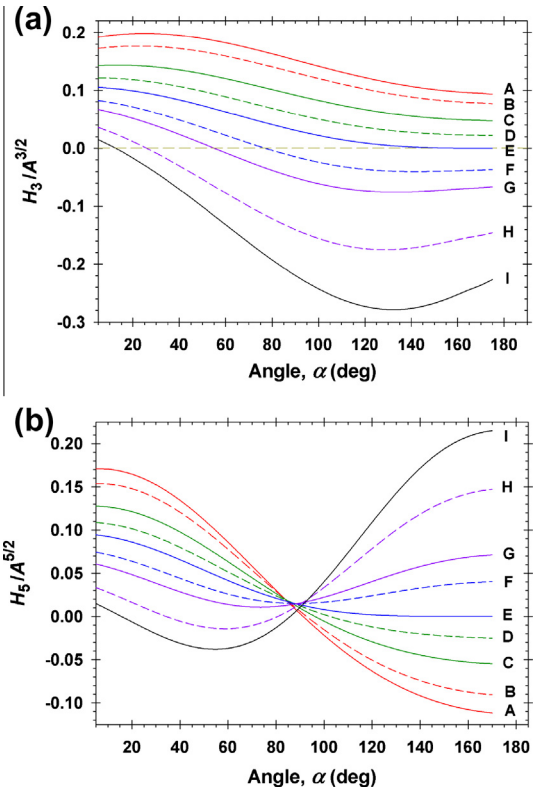

Fig. 7. Dependence of the scaled coefficient functions (a) $H_3(\alpha, \varepsilon_{pn})/A^{3/2}$ and (b) $H_5(\alpha, \varepsilon_{pn})/A^{5/2}$ on the central angle, α, at different fixed values of ε_{pn}: (A) 0.125; (B) 0.250; (C) 0.500; (D) 0.750; (E) 1.00; (F) 1.50; (G) 2.00; (H) 4.00; (I) 8.00.

The renormalizing factor A is defined by Eq. (4.15). As seen in Fig. 7a, H_3 monotonically decreases with the rise of ε_{pn}. The behavior of H_5 is more complicated (Fig. 7b). For hydrophilic particles ($\alpha < 90°$), H_5 decreases with the rise of ε_{pn}, whereas for hydrophobic particles ($\alpha > 90°$), H_5 increases with the rise of ε_{pn}.

The integrable singularity of E_z at the contact line on the particle surface gives an essential contribution to the normal (electrodipping) force acting on the particle; see Section 6. For this reason, it is necessary to accurately estimate the coefficient function $J_{E1}(\alpha, \varepsilon_{pn})$ defined by Eq. (3.22). The most convenient formula for calculating $J_{E1}(\alpha, \varepsilon_{pn})$, which is derived in Appendix A, is as follows:

$$J_{E1} = J_{E1}^{(0)} + \frac{2^{1/2-\nu} A_E}{\pi^{1/2}\nu} \frac{\Gamma(0.5+\nu)}{\Gamma(\nu)} \tag{5.7}$$

where ν is the first positive root ($0.5 < \nu < 1$) of the equation (see Table 1 in Appendix B)

$$\sin[(2\pi-\alpha)\nu] = \beta \sin(\alpha\nu); \tag{5.8}$$

$$J_{E1}^{(0)} = \left\{\frac{2\beta}{3}[\cot\alpha \sin(\alpha\nu) + 2\nu\cos(\alpha\nu)] - (1+\beta)\frac{\nu\sin[(\pi-\alpha)\nu]}{\sin(\pi\nu)}\right\} \times \frac{2^{2-\nu}\pi^{1/2}}{(2\pi-\alpha)\cos[(2\pi-\alpha)\nu] - \beta\alpha\cos(\alpha\nu)} \frac{\Gamma(0.5+\nu)}{\Gamma(\nu)}; \tag{5.9}$$

$$A_E = \lim_{y\to\infty}\left\{\exp(\nu y)\int_0^\infty \frac{\tau\Psi_b^{(1)}(\tau)\coth(\pi\tau)}{\sinh[(\pi-\alpha)\tau]}\sin(\tau y)d\tau\right\}. \tag{5.10}$$

$\Psi_b^{(1)}(\tau)$ is defined by Eq. (A.41) in Appendix A. The limit in Eq. (5.10) is calculated numerically using the $\Psi_b(\tau)$ dependence obtained as

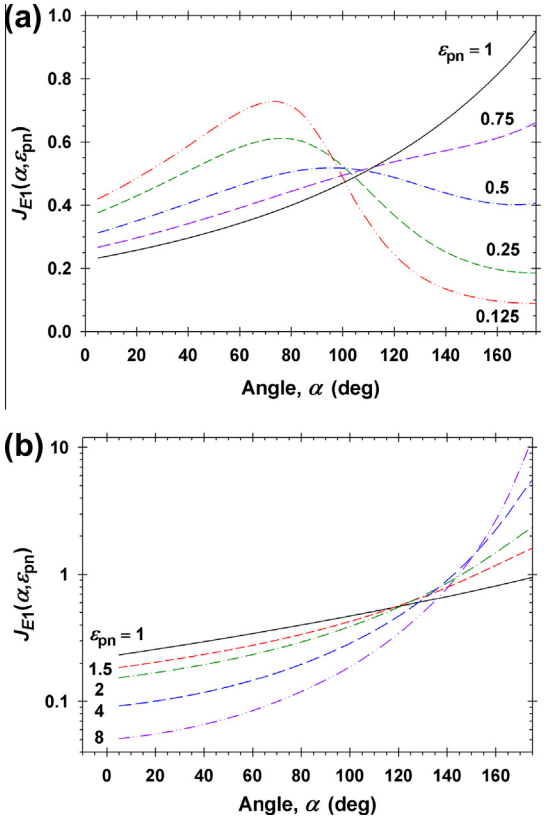

Fig. 8. Dependence of the coefficient function $J_{E1}(\alpha, \varepsilon_{pn})$ on the central angle α for different values of the ratio $\varepsilon_{pn} = \varepsilon_p/\varepsilon_n$. At $\varepsilon_{pn} = 1$, the calculated curve coincides with that in Fig. 3.

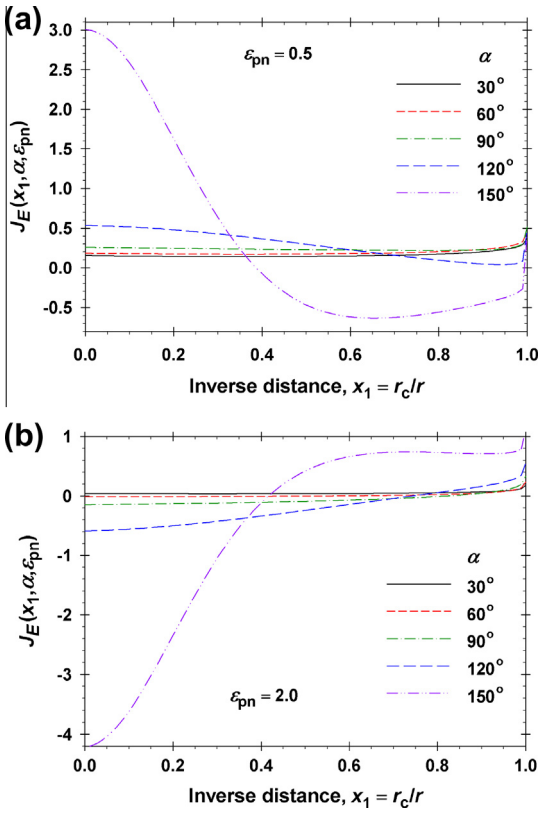

Fig. 9. Dependence of the coefficient function $J_E(x_1, \alpha, \varepsilon_{pn})$ in the expression for E_z, Eq. (3.20), on x_1 for different values of the central angle α at (a) $\varepsilon_{pn} = 0.5$ and (b) $\varepsilon_{pn} = 2$.

explained in Section 5.1 and Appendix A. The calculated values of J_{E1} are plotted in Fig. 8 and tabulated in Table 2 of Appendix B.

Our numerical calculations showed that the last term in Eq. (5.7) is small (on order of 10%), so that one can set $J_{E1} \approx J_{E1}^{(0)}$, except for $\alpha > 170^{o}$. Therefore, for a fast estimation of J_{E1}, one can use the analytical exact expression, Eq. (5.9).

In the limiting case $\beta \to 0$ ($\varepsilon_{pn} \to 1$), Eq. (5.8) gives $v \to v_e$, where v_e is defined by Eq. (4.7), and then Eq. (5.9) reduces to Eq. (4.8). In the same limiting case, $A_E \to 0$; see Appendix A.

Finally, Fig. 9 shows the dependence of the coefficient function $J_E(x_1, \alpha, \varepsilon_{pn})$ in the expression for E_z, Eq. (3.20), on x_1 at various central angles, α, and at two ε_{pn} values. The results show that J_E vs. x_1 is almost constant, except for $\alpha > 120^{\circ}$ and in a close vicinity of the contact line, $x_1 \to 1$. The limiting values of J_E for $x_1 = 1$ are given by J_{E1} in Fig. 8.

6. Electrodipping force

6.1. Theoretical expressions and numerical results

As before, we consider a single particle attached to a water–nonpolar fluid interface in the presence of applied uniform electric field $\mathbf{E}_0$, which is parallel to the vertical axis z (Fig. 1). In Part 2 of the present study [45], it is proven that the electric force acting on the particle is given by the expression:

$$\mathbf{F} = -\mathbf{e}_z \frac{\varepsilon_n}{8\pi} \int_{S_{nw}} (E_z^2 - E_0^2) dS. \tag{6.1}$$

Here, $\mathbf{e}_z$ is the unit vector of the z-axis. In the absence of external force ($E_0 = 0$), the force $\mathbf{F}$ is directed downwards, toward the phase of greater dielectric constant (the water), and for this reason, it was called electrodipping force [48]. Eq. (6.1) is derived by integrating the divergence of the Maxwell electric stress tensor over the spatial domain of the nonpolar fluid and by application of the Gauss-Ostrogradsky theorem. Thus, one obtains that the integral over the particle upper surface S_{pn} is equal to the integral over the flat water-nonpolar fluid interface S_{nw} in Eq. (6.1); see [45].

Substituting E_z from Eq. (3.12) into Eq. (6.1) and using Eq. (2.7), we obtain an expression for the normal (electrodipping) force:

$$F^{(n)} \equiv F_z = -\frac{\varepsilon_n E_0^2 R^2}{4\pi} f_{R,EE}, \tag{6.2}$$

where

$$f_{R,EE} \equiv \pi \sin^2\alpha \int_0^{\infty} [2 + (\cosh\eta - 1)^{3/2} I_E] \frac{I_E \sinh\eta d\eta}{(\cosh\eta - 1)^{1/2}}. \tag{6.3}$$

With the help of Eqs. (3.13) and (3.14), we introduce x_1 as integration variable. Because the integrand has an integrable singularity, it is convenient to represent Eq. (6.3) in the form:

$$f_{R,EE} = \pi \sin^2\alpha \left\{ \int_0^{1-\delta} \left[2\left(\frac{2}{1-x_1^2}\right)^{3/2} I_E + x_1^3 \left(\frac{2}{1-x_1^2}\right)^3 I_E^2 \right] dx_1 + f_{\delta,EE} \right\}, \tag{6.4}$$

where in view of Eq. (3.22), the integration in $f_{\delta,EE}$ can be carried out analytically:

$$f_{\delta,EE} \approx \int_{1-\delta}^{1} [2(1-x_1)^{v-1} J_{E1} + (1-x_1)^{2v-2} J_{E1}^2] dx_1 = \frac{2\delta^v}{v} J_{E1} + \frac{\delta^{2v-1}}{2v-1} J_{E1}^2. \tag{6.5}$$

A good accuracy can be obtained setting $\delta = 0.01$. The integral in Eq. (6.4) can be solved numerically using the calculated $J_E(x_1, \alpha, \varepsilon_{pn})$; see Eq. (3.20) and Fig. 9.

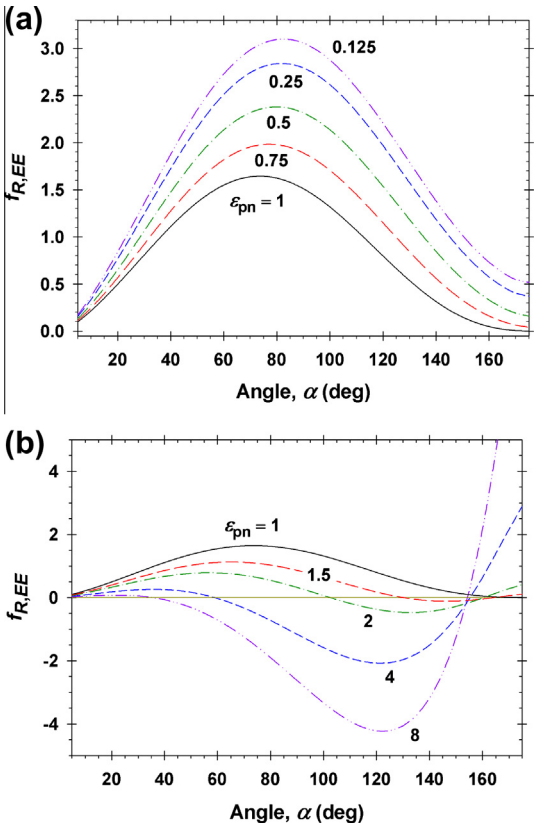

Fig. 10. Dependence of the force coefficient $f_{R,EE}$ on the central angle α at different fixed values of the dielectric constant ratio, $\varepsilon_{pn} = \varepsilon_p/\varepsilon_n$.

Calculated values of $f_{R,EE}$ are given in Table 5 of Appendix B and shown in Fig. 10. It is interesting that for $\varepsilon_{pn} > 1$, there are regions of α values, where $f_{R,EE}$ is negative. In these regions, F_z is positive, i.e., the electric force pushes the particle upwards, toward the nonpolar fluid.

Fig. 11 illustrates the sign and magnitude of F_z depending on the applied electric field E_0 for a hydrophilic particle with $\alpha = 60^{\circ}$ (Fig. 11a) and for a hydrophobic particle with $\alpha = 120^{\circ}$ (Fig. 11b). In accordance with Eq. (6.2), the F_z-vs.-E_0 curves in Fig. 11 are parabolas passing through the coordinate origin, i.e., $F_z = 0$ for $E_0 = 0$. This is related to the fact that here we consider uncharged particles, for which F_z is due to the external field and to the fact that the particle, in general, has a dielectric constant that is different from those of the two adjacent phases. In addition, the F_z-vs.-E_0 dependences are symmetric and insensitive of whether E_0 is positive and negative. If the respective experimental dependence is asymmetric, this will indicate that the particle is charged; see Ref [45].

For the *hydrophilic* particle (Fig. 11a), F_z dips the particle into the water for $\varepsilon_{pn} < 4$ and pulls the particle upwards for $\varepsilon_{pn} \geqslant 4$. For the *hydrophobic* particle (Fig. 11b), the transition between dipping and pulling F_z occurs for ε_{pn} between 1 and 2.

6.2. Tabulated values of the computed basic functions

For a fast and convenient application of the results obtained in the present paper, the reader could use the dependencies, $v(\alpha, \varepsilon_{pn})$, $J_{E1}(\alpha, \varepsilon_{pn})$, $H_3(\alpha, \varepsilon_{pn})$, $H_5(\alpha, \varepsilon_{pn})$ and $f_{R,EE}(\alpha, \varepsilon_{pn})$ given in Tables 1–5 in Appendix B, instead of repeating the calculations described in the text.

Let $f(\alpha, \varepsilon_{pn})$ be either of the above tabulated functions. We are interested to obtain its value for a given $\alpha_1 < \alpha < \alpha_2$, and $\varepsilon_1 < \varepsilon_{pn} <$

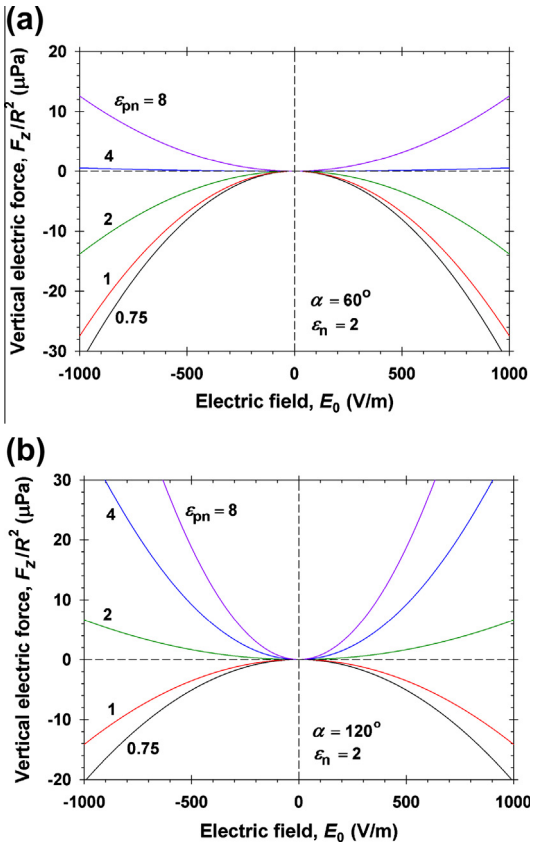

Fig. 11. Plot of the vertical electric force F_z (divided by R^2) vs. the applied external electric field, E_0, (a) for a hydrophilic particle with $\alpha = 60°$, and (b) for a hydrophobic particle with $\alpha = 120°$. In both cases, the dielectric constant of the nonpolar fluid is the same, $\varepsilon_n = 2$ (e.g., oil), whereas that of the particle, ε_p, is different for the different curves; $\varepsilon_{pn} = \varepsilon_p/\varepsilon_n$.

ε_2, where α_1, α_2, ε_1 and ε_2 are values given in the respective table. Then, $f(\alpha, \varepsilon_{pn})$ can be calculated by means of the following four-point interpolation formula:

$$f(\alpha,\varepsilon_{pn}) = \frac{(\alpha-\alpha_2)(\varepsilon_{pn}-\varepsilon_2)}{(\alpha_1-\alpha_2)(\varepsilon_1-\varepsilon_2)} f(\alpha_1,\varepsilon_1) + \frac{(\alpha-\alpha_2)(\varepsilon_{pn}-\varepsilon_1)}{(\alpha_1-\alpha_2)(\varepsilon_2-\varepsilon_1)} f(\alpha_1,\varepsilon_2) + \frac{(\alpha-\alpha_1)(\varepsilon_{pn}-\varepsilon_2)}{(\alpha_2-\alpha_1)(\varepsilon_1-\varepsilon_2)} f(\alpha_2,\varepsilon_1) + \frac{(\alpha-\alpha_1)(\varepsilon_{pn}-\varepsilon_1)}{(\alpha_2-\alpha_1)(\varepsilon_2-\varepsilon_1)} f(\alpha_2,\varepsilon_2) \tag{6.6}$$

7. Asymptotic expression for the lateral electric force between two particles

7.1. Multipole expansion at long distances

Here, we are using the solution of the single-particle problem to derive an expression for the force of interaction between two particles at sufficiently long distances between them. Let us consider two identical particles, attached to the water-nonpolar fluid interface, at distance L between the centers of their contact lines (Fig. 12). As before, an external electric field $\mathbf{E}_0$ is applied normal to the interface. The external field polarizes the floating particles, which leads to electrostatic interaction between them. In view of Eq. (3.12), the electric potential in the nonpolar fluid can be presented in the form:

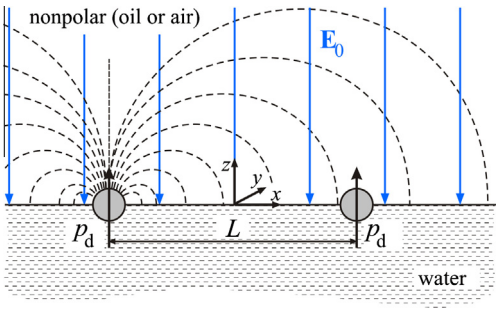

Fig. 12. Sketch of two uncharged dielectric particles attached to the water-nonpolar fluid interface and separated at a distance L. The applied uniform external electric field $\mathbf{E}_0$ polarizes the particles. Far from each particle, its electric field is equivalent to the field of a dipole of moment p_d given by Eq. (7.5).

$$\varphi_n \equiv E_0 z + \tilde{\varphi}_n, \tag{7.1}$$

where $E_0 z$ and $\tilde{\varphi}_n$ are, respectively, the contributions of the external field and of the polarized particles. As before, the penetration of the electric field in the lower phase of greater dielectric constant (the water phase) is neglected, which is possible for particle radius $R \gg \kappa^{-1}$, where κ is the Debye screening parameter for this phase [48]. As proven in Part 2 of this study [45], under such conditions the force of electrostatic interaction between the two floating particles can be calculated from the expression:

$$F_{12} \equiv F_x^{(el)} = \frac{\varepsilon_n}{8\pi}\int_{-\infty}^{\infty} dy \int_0^{\infty} dz \left[\left(\frac{\partial\tilde{\varphi}_n}{\partial y}\right)^2 + \left(\frac{\partial\tilde{\varphi}_n}{\partial z}\right)^2\right] \text{ at } x = 0. \tag{7.2}$$

Here, the x-axis passes through the centers of the contact lines of the two particles; $F_x^{(el)}$ is the x-projection of the force exerted on the right-hand-side particle; the coordinate origin is fixed in the middle between the two particles; the y- and z-axes have, respectively, horizontal and vertical orientation (Fig. 12). The integration in Eq. (7.2) is carried out throughout the vertical yz-plane in the middle between the two particles. Eq. (7.2) shows that $F_x^{(el)} \geq 0$, i.e., the electrostatic interaction between the two particles is repulsion.

At sufficiently long distances between the two particles, the electric potential $\tilde{\varphi}_n$ can be presented as a superposition of the electric potentials created by the individual particles:

$$\tilde{\varphi}_n \approx \tilde{\varphi}_{n,A} + \tilde{\varphi}_{n,B}. \tag{7.3}$$

Here and hereafter, the subscripts A and B denote quantities related, respectively, to the left- and right-hand-side particle. In view of the asymptotic expansion Eq. (3.17), we can represent Eq. (7.3) in the form:

$$\tilde{\varphi}_{n,k} = \frac{p_d}{\varepsilon_n}\frac{z}{(r_k^2+z^2)^{3/2}} + \frac{p_o}{\varepsilon_n}\left[\frac{z}{(r_k^2+z^2)^{5/2}} - \frac{5z^3}{3(r_k^2+z^2)^{7/2}}\right] \quad (k = A, B), \tag{7.4}$$

where the first term arises from the Legendre polynomial P_1 (dipolar term) and the second one from the Legendre polynomial P_3 (octupolar term) [65]; the dipolar and octupolar moments, p_d and p_o, are defined as follows:

$$p_d \equiv \varepsilon_n E_0 H_3 r_c^3 \quad \text{and} \quad p_o \equiv \varepsilon_n E_0 H_5 r_c^5 \tag{7.5}$$

where $H_3(\alpha, \varepsilon_{pn})$ and $H_5(\alpha, \varepsilon_{pn})$ are coefficient functions defined by Eqs. (3.18) and (3.19), tabulated in Tables 3 and 4 of Appendix B, and plotted in Fig. 7. The radial distances, r_A and r_B, are defined by the relationships

$$r_A^2 \equiv \left(x + \frac{L}{2}\right)^2 + y^2 \quad \text{and} \quad r_B^2 \equiv \left(x - \frac{L}{2}\right)^2 + y^2. \tag{7.6}$$

The substitution of Eqs. (7.3) and (7.4) into Eq. (7.2) yields:

$$F_x^{(el)} \approx -\frac{1}{32\pi\varepsilon_n}\int_{-\infty}^{\infty}\int_{0}^{\infty} U_x(y,z)dzdy, \tag{7.7}$$

where U_x is given by the expression:

$$\begin{aligned} U_x(y,z) \equiv \{&16y^2z^2[9p_d(L^2+4y^2+4z^2)^2+20p_o(3L^2+12y^2\\ &-16z^2)]^2+[3p_d(L^2+4y^2+4z^2)^2(L^2+4y^2-8z^2)\\ &+4p_o(3L^4+24L^2y^2-96L^2z^2+48y^4-384y^2z^2\\ &+128z^4)]^2\}\frac{1}{9(L^2+4y^2+4z^2)^9}. \end{aligned} \tag{7.8}$$

The integral in Eq. (7.7) can be taken analytically; the final result is:

$$F_x^{(el)} \approx \frac{1}{\varepsilon_n L^4}\left(\frac{3}{2}p_d^2+\frac{5p_dp_o}{L^2}+\frac{175p_o^2}{18L^4}\right). \tag{7.9}$$

For $p_d \neq 0$, the leading term is the dipolar term, and then, the long-distance asymptotics of the electrostatic interaction force is [4,5,23]:

$$F_x^{(el)} \approx \frac{3p_d^2}{2\varepsilon_n L^4}. \tag{7.10}$$

For special values of the central angle α and the dielectric constant ratio ε_{pn}, the coefficient function $H_3(\alpha, \varepsilon_{pn})$ becomes equal to zero, and then $p_d = 0$; see Fig. 7a and Eq. (7.5). In such a case, the octupolar term becomes the leading term in Eq. (7.9), so that the interaction force becomes:

$$F_x^{(el)} \approx \frac{175p_o^2}{18\varepsilon_n L^8}. \tag{7.11}$$

In the latter case, the direct electrostatic repulsion, $F_x^{(el)} \propto 1/L^8$, decays much faster than the electrocapillary attraction, $F_x^{(EC)} \propto 1/L^4$ [3–5], so that the net force is attractive at long distances.

In the considered case of uncharged particles, the dipolar and octupolar moments, p_d and p_o, are induced by the applied external field and therefore both of them vanish at $E_0 \to 0$; see Eq. (7.5).

Note also that if $p_d \neq 0$ and the exact method of reflections [66] is used, instead of the superposition approximation, Eq. (7.3), an additional octupolar term $\propto p_d^2/L^8$ will appear in Eq. (7.9). However, for $p_d \neq 0$, the octupolar terms are negligible and the asymptotic force is given by Eq. (7.10). Conversely, if $p_d = 0$, the term $\propto p_d^2/L^8$ disappears, and the leading term is the octupolar term given by Eq. (7.11) because, in general, $H_5(\alpha, \varepsilon_{pn})$ is not equal to zero when $H_3(\alpha, \varepsilon_{pn}) = 0$; see Fig. 7a and b.

7.2. Numerical results and discussion

To compute $F_x^{(el)}$ for various E_0, α and ε_{pn}, we used Eqs. (7.5) and (7.9), along with the calculated coefficient functions $H_3(\alpha, \varepsilon_{pn})$ and $H_5(\alpha, \varepsilon_{pn})$. The values of the latter functions can be obtained using the interpolation formula in Eq. (6.6) and the data tabulated in Tables 3 and 4 of Appendix B.

Fig. 13a and b show plots of $F_x^{(el)}/R^2$ vs. E_0, for different values of the central angle, α, at a fixed interparticle distance $L = 6R$. For the dielectric constants, we have used experimental values for tetradecane and glass particles from Ref. [48], viz. $\varepsilon_n = 2.04$ and $\varepsilon_p = 3.97$. For $55° \leqslant \alpha \leqslant 150°$, $F_x^{(el)}$ strongly diminishes with the decrease in α. In particular, for hydrophobic particles, $F_x^{(el)}$ is by orders of magnitude greater than for hydrophilic particles; compare Fig. 13a and b. $H_3 = 0$ at $\alpha \approx 55°$ and in this case $F_x^{(el)}$ is dominated by the octupolar term, see Eq. (7.11). For this reason, $F_x^{(el)}$ has a minimal value at $\alpha = 55°$.

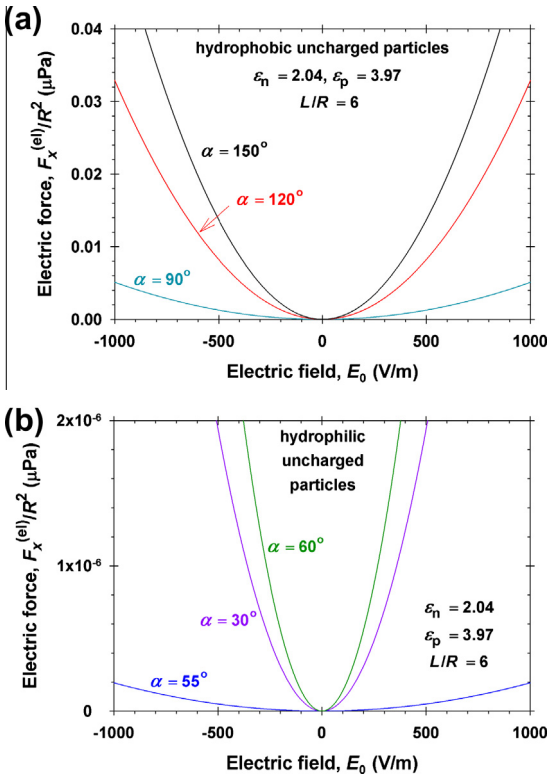

Fig. 13. Plots of $F_x^{(el)}/R^2$ vs. the applied external field, E_0, for different values of the central angle, α, at a fixed interparticle distance $L = 6R$; (a) hydrophobic uncharged particles; (b) hydrophilic uncharged particles.

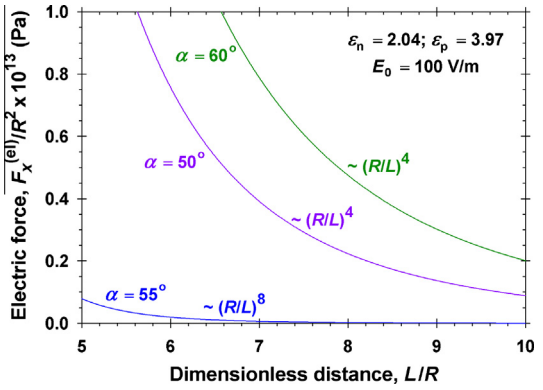

Fig. 14. Plots of $F_x^{(el)}/R^2$ vs. the scaled interparticle distance, L/R, at external field $E_0 = 100$ V/m for three values of the central angle, α. At $\alpha = 50°$ and 60°, the force is dominated by the dipolar interaction, Eq. (7.10), whereas at $\alpha = 55°$ – by the octupolar interaction, Eq. (7.11).

The diminishing of $F_x^{(el)}$ with the decrease in α (Fig. 13) is partially due to the fact that the external electric field, which polarizes the dielectric particle, enters the particle through the surface S_{pn} (Fig. 1), but S_{pn} considerably decreases with the decrease in α.

Fig. 14 shows $F_x^{(el)}/R^2$ vs. the dimensionless distance L/R at $E_0 = 100$ V and at three α values. At $\alpha = 50°$ and 60°, the dipolar term is predominant and $F_x^{(el)} \propto 1/L^{-4}$; see Eq. (7.10). In contrast, at $\alpha = 50°$, the dipolar term is zero ($p_d = 0$) and we are dealing with octupole–octupole interaction, $F_x^{(el)} \propto 1/L^{-8}$; see Eq. (7.11). In this case, the attractive electrocapillary force, $F_x^{(EC)} \propto 1/L^4$ [3–5], dominates the interparticle force, at least at long distances.

8. Discussion

Here, we give a physical interpretation of the results obtained by solving the mathematical boundary problem.

8.1. Inversion of the direction of particle dipole moment

As seen in Fig. 7a, for a given $\varepsilon_{pn} > 1$, the coefficient function H_3 can change its sign at a certain value of the contact angle α. The same is true for the particle dipole moment, $p_d \sim H_3$, which is induced by the external field, see Eqs. (3.17) and (7.5). At this special value of α, corresponding to a certain degree of particle immersion in the water phase, we have $H_3 = 0$ and $p_d = 0$, and then, the interparticle force $F_x^{(el)}$ is dominated by the octupolar term; see Eqs. (7.9) and (7.11). In contrast, for $\varepsilon_{pn} < 1$, the coefficient H_3 is positive for all α, and sign inversion of p_d is absent (Fig. 7a).

This behavior can be explained on the basis of the fact that p_d is an excess dipole moment. If we consider a dielectric particle in vacuum, the external field $\mathbf{E}_0$ induces polarization charges on the particle surface, which give rise to an additional electric field inside the particle that is directed oppositely to $\mathbf{E}_0$. By definition, in such a case, the polarization vector and the intergral particle dipole moment, $\mathbf{p}_d$, have the same direction as $\mathbf{E}_0$ [67]. However, if the particle is immersed in a fluid of greater dielectric constant (instead of vacuum), then the particle polarization will be smaller than that of the same volume of the fluid. In such a case, the vector of excess polarization and particle dipole moment, $\mathbf{p}_d$, has a direction opposite to $\mathbf{E}_0$.

First, let us consider the case $\varepsilon_{pn} = \varepsilon_p/\varepsilon_n < 1$ (Fig. 15a). In this case, both the upper and the lower portions of the particle are immersed in a medium of greater dielectric constant, so that the respective excess dipole moments, denoted $\mathbf{p}_{d,1}$ and $\mathbf{p}_{d,2}$ in Fig. 15a, are directed opposite to $\mathbf{E}_0$. (The water phase is assumed to have the greatest dielectric constant among the three neighboring phases.) In such a case, the dipole moments $\mathbf{p}_{d,1}$ and $\mathbf{p}_{d,2}$ cannot annihilate each other; the net dipole moment $\mathbf{p}_d$ cannot become zero, and H_3 can be only positive (Fig. 7a).

For $\varepsilon_{pn} > 1$ (Fig. 15b), the upper portion of the particle is immersed in a fluid of lower dielectric constant, whereas the lower portion – in a fluid of greater dielectric constant. In such a case, $\mathbf{p}_{d,1}$ has the same direction as $\mathbf{E}_0$, whereas $\mathbf{p}_{d,2}$ has the opposite direction. At a given contact angle α, we can have $\mathbf{p}_{d,1} + \mathbf{p}_{d,2} = 0$, which corresponds to $H_3 = 0$ and to zero net particle dipole moment, p_d. At the smaller α, the particle is immersed deeper in the water, the effect of $\mathbf{p}_{d,2}$ prevails and we have $H_3 > 0$, as for $\varepsilon_{pn} < 1$ (Fig. 7a). Conversely, at the larger α, the effect of $\mathbf{p}_{d,1}$ prevails and we have $H_3 < 0$.

8.2. Inversion of the sign of electrodipping force

Here, our goal is to give a physical interpretation of the sign of the coefficient $f_{R,EE}$, which determines the direction of the vertical force, F_z; see Fig. 10 and Eq. (6.2).

For $\varepsilon_{pn} = \varepsilon_p/\varepsilon_n < 1$ (Fig. 15a), the polarization charges at the bottom of the particle, which is immersed in water, are neutralized by counterions that are attracted from the aqueous phase, whereas the excess polarization charges at the top particle surface have the same sign as that on the electrode above the particle. In such a case, the electrode (that creates $\mathbf{E}_0$) repels the particle and pushes it toward the water phase. Correspondingly, $f_{R,EE}$ is positive (Fig. 10a).

For $\varepsilon_{pn} > 1$ (Fig. 15b), at sufficiently small angle α, the effect of $\mathbf{p}_{d,2}$ prevails and we have the same situation as that described in the previous paragraph. This corresponds to the fact that $f_{R,EE}$ is positive for the smaller α in Fig. 10b.

For $\varepsilon_{pn} > 1$, at the greater α, the effect of $\mathbf{p}_{d,1}$ becomes predominant. Then, the particle energy in the external field decreases if the portion of the particle immersed in water decreases. Consequently, the particle is attracted by the electrode, and $f_{R,EE}$ is negative at the intermediate α values in Fig. 10b.

Finally, at $\varepsilon_{pn} > 1$ and $\alpha > 160°$, $f_{R,EE}$ becomes positive again (Fig. 10b). This attraction of the particle by the water phase could be attributed to the attraction between the polarization charges at the particle surface and the counterions at the water surface across the wedge-shaped region around the particle bottom (Fig. 15c). Because the electric field does not penetrate in the aqueous phase, each force line in the nonpolar fluid must end at a charge (counterion) located at the nonpolar-fluid/water interface, as sketched in Fig. 15c. At smaller α, the wedge-shaped region disappears, and $f_{R,EE}$ becomes negative (Fig. 10b).

The considerations in this section have a qualitative character. Their only purpose to give a physical interpretation of the zeros and sign changes of H_3 and $f_{R,EE}$, as well as of F_z and $F_x^{(el)}$. However, these considerations cannot replace the exact solution of the problem presented in Sections 2–7. For convenience, the procedures for exact calculation of F_z and $F_x^{(el)}$ are presented in Table 1.

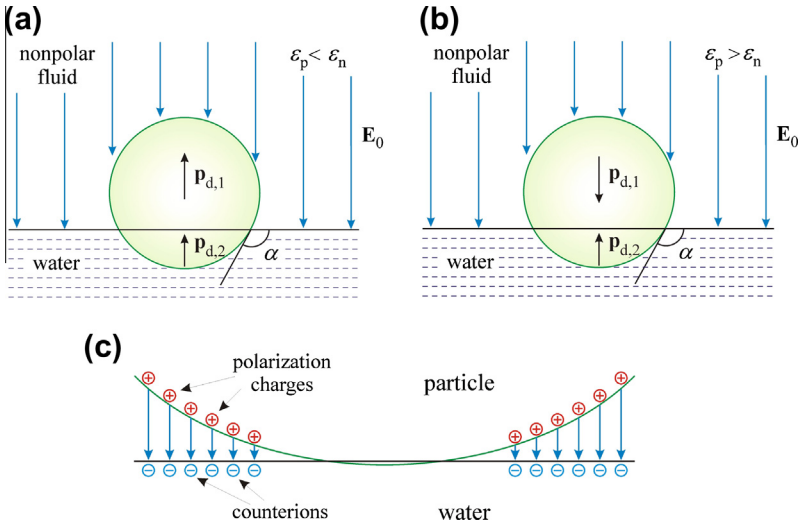

Fig. 15. Sketch of a particle at a water/nonpolar-fluid interface in external field $\mathbf{E}_0$. (a) In the case $\varepsilon_p < \varepsilon_n$, the induced excess dipole moments of the upper and lower portions of the particle, $\mathbf{p}_{d,1}$ and $\mathbf{p}_{d,2}$, have the same directions, (b) in the case $\varepsilon_p > \varepsilon_n$, the excess dipole moments $\mathbf{p}_{d,1}$ and $\mathbf{p}_{d,2}$ have the opposite directions and (c) attraction between polarization charges and counterions across the wedge-shaped region around the zone of particle contact with the water phase.

Table 1
Procedures for calculation of the vertical (electrodipping) force F_z acting on a single particle and of the lateral force $F_x^{(el)}$ between two particles.

Step	Calculation of F_z
1	Input parameters: E_0, R, α, ε_p, ε_n, and $\varepsilon_{pn} = \varepsilon_p/\varepsilon_n$
2	Calculate $f_{R,EE}(\alpha, \varepsilon_{pn})$ using Eq. (6.6) and Table 5 in Appendix B
3	Calculation of F_z from Eq. (6.2)
	Calculation of $F_x^{(el)}$
4	Input parameters: the same as in point 1, plus L and $r_c = R\sin\alpha$
5	Calculate $H_3(\alpha, \varepsilon_{pn})$ and $H_5(\alpha, \varepsilon_{pn})$ using Eq. (6.6) and Tables 3 and 4 in Appendix B
6	Calculate p_d and p_o from Eq. (7.5)
7	Calculate $F_x^{(el)}$ from Eq. (7.9)

9. Conclusions

In this study, we address the problem for calculating the electric forces acting on uncharged dielectric colloidal particles, which are attached to the interface between a nonpolar fluid (air, oil) and water in the presence of applied uniform external electric field. The final goal is to calculate the normal (electrodipping) force acting on each separate particle, and the force of interaction between two identical particles. As demonstrated above, these forces exhibit interesting non-monotonic dependences on the particle contact angle. The problem is important because of the potential use of electric fields for controlling the distances between particles in non-densely packed interfacial colloidal crystals for obtaining lithographic masks used in the production of antireflective coatings, microlens arrays, etc. [30–33]. The case of charged particles in external field is considered in the second part of this study [45].

An uncharged particle experiences the action of electric forces because of the polarization of the particle by the external field. Our main task is to find the electric field inside the particle and in the nonpolar fluid around it. As demonstrated in a previous study [1], at such geometry an exact analytical solution can be obtained by solving the Laplace equation in toroidal coordinates and separating the variables by means of the Mehler–Fock integral transform. To calculate the electric forces acting on the particle it is enough to find the normal component of the electric field at the water-nonpolar fluid interface, viz. $E_{z|z=0}$. The effect of the integrable singularity of E_z at the particle three-phase contact line was accurately taken into account (Fig. 8), because this effect gives a finite contribution to the normal (electrodipping) force, F_z.

At a given particle radius, R, the magnitude and sign of F_z is affected by three parameters: the applied electric field, E_0, the particle contact angle, α, and the ratio of the dielectric constants of the particle and nonpolar fluid, $\varepsilon_{pn} = \varepsilon_p/\varepsilon_n$. The magnitude of F_z increases $\propto E_0^2$. The dependence of F_z on α and ε_{pn} is quite non-trivial. For $\varepsilon_{pn} \leqslant 1$, the electrodipping force depends non-monotonically on the immersion depth and has a maximum (Fig. 10a). More interestingly, for $\varepsilon_{pn} > 1$, the dependence of F_z on the contact angle α exhibits a maximum and a minimum. F_z can be either negative (dipping), positive (pulling), or zero, depending on the value of α (Fig. 10b); see Section 8b for physical interpretation.

The particle dipolar moment p_d, induced by the external field, can become zero if the particle dielectric constant ε_p is intermediate between those of the nonpolar fluid and water, $\varepsilon_n < \varepsilon_p < \varepsilon_w$. In such a case, the excess polarizations of the upper and lower portions of the particle (with respect to those of the displaced fluids) have the opposite signs and can annihilate each other at a given contact angle α. At this special value of α, which depends on the ratio $\varepsilon_p/\varepsilon_n$, the dipolar interaction disappears ($p_d = 0$) and then the electrostatic force between two uncharged floating particles, $F_x^{(el)}$, is dominated by the octupolar term; see Eqs. (7.9) and (7.11). It should be noted that the multipole expansion of the electric field has dipolar and octupolar terms, with zero quadrupolar term; see Eqs. (3.17) and (7.4).

If the dipolar term is zero, and the lateral repulsive force is determined by the octupolar term, the interparticle repulsion drops by orders of magnitude and decays much faster with the interparticle distance. Then, the attractive lateral capillary forces and the van der Waals forces can overcome the electrostatic repulsion and can induce two-dimensional coagulation of the particles at the interface. In general, the dipolar part of the lateral force $F_x^{(el)}$ and the normal force F_z become equal to zero at different values of α, so that an electric-field induced capillary meniscus (engendered by F_z) can appear around the particle even if its electric dipolar moment is zero ($F_x^{(el)} \approx 0$).

The results in the present article are obtained assuming that the particle radius is much greater than the Debye screening length in the water phase, $\kappa R \gg 1$. In such a case, the electrostatic interactions across the water phase are negligible and only the electric effects in the nonpolar fluid and inside the dielectric particle are essential. This study could be further extended to smaller particles, for which $\kappa R \leqslant 1$. Other directions for further developments are (i) to take into account the electric-field-induced lateral capillary force, as in Ref. [3]; (ii) to replace the water with a second nonpolar fluid, e.g., air-oil interface as in the experiments in Refs. [17,18]; (iii) to theoretically examine the effects of alternating electric field, and (iv) to compare the theoretical predictions with the experiment.

Acknowledgments

The authors gratefully acknowledge the support from the National Science Fund of Bulgaria, Grant No. DO-02-121/2009; from the FP7 project Beyond-Everest, and from the ESF COST Action CM1101.

Appendix A. Supplementary material

Supplementary data associated with this article can be found, in the online version, at http://dx.doi.org/10.1016/j.jcis.2013.05.020.

References

[1] K.D. Danov, P.A. Kralchevsky, J. Colloid Interface Sci. 298 (2006) 213–231.
[2] K.D. Danov, P.A. Kralchevsky, M.P. Boneva, Langmuir 22 (2006) 2653–2667.
[3] K.D. Danov, P.A. Kralchevsky, J. Colloid Interface Sci. 345 (2010) 505–514.
[4] A. Würger, L. Foret, J. Phys. Chem. B 109 (2005) 16435–16438.
[5] A. Domínguez, M. Oettel, S. Dietrich, J. Chem. Phys. 127 (2007) 204706.
[6] B.J. Park, J.P. Pantina, E.M. Furst, M. Oettel, S. Reynaert, J. Vermant, Langmuir 24 (2008) 1686–1694.
[7] M.P. Boneva, K.D. Danov, N.C. Christov, P.A. Kralchevsky, Langmuir 25 (2009) 9129–9139.
[8] M.P. Boneva, N.C. Christov, K.D. Danov, P.A. Kralchevsky, Phys. Chem. Chem. Phys. 9 (2007) 6371–6384.
[9] D. Stamou, C. Duschl, D. Johannsmann, Phys. Rev. E 62 (2000) 5263–5272.
[10] T.S. Horozov, R. Aveyard, B.P. Binks, J.H. Clint, Langmuir 21 (2005) 7405–7412.
[11] T.S. Horozov, B.P. Binks, Colloids Surf., A 267 (2005) 64–73.
[12] E.P. Lewandowski, J.A. Bernate, P.C. Searson, K.J. Stebe, Langmuir 24 (2008) 9302–9307.
[13] E.P. Lewandowski, M. Cavallaro, L. Botto, J.C. Bernate, V. Garbin, K.J. Stebe, Langmuir 26 (2010) 15142–15154.
[14] P.A. Kralchevsky, N.D. Denkov, K.D. Danov, Langmuir 17 (2001) 7694–7705.
[15] K.D. Danov, P.A. Kralchevsky, B.N. Naydenov, G. Brenn, J. Colloid Interface Sci. 287 (2005) 121–134.
[16] K.D. Danov, P.A. Kralchevsky, Adv. Colloid Interface Sci. 154 (2010) 91–103.
[17] N. Aubry, P. Singh, Phys. Rev. E 77 (2008) 056302.
[18] N. Aubry, P. Singh, M. Janjua, S. Nudurupati, Proc. Natl. Acad. Sci. USA 105 (2008) 3711–3714.
[19] M. Janjua, S. Nudurupati, P. Singh, N. Aubry, Mech. Res. Commun. 36 (2009) 55–64.
[20] P. Singh, D.D. Joseph, N. Aubry, Soft. Matter. 6 (2010) 4310–4325.
[21] P. Singh, M. Hossain, B. Dalal, S.K. Gurupatham, I.S. Fischer, Mech. Res. Commun. 45 (2012) 54–57.
[22] K. Masschaele, J. Vermant, Soft. Matter. 7 (2011) 10597–10600.
[23] R. Aveyard, J.H. Clint, D. Nees, V.N. Paunov, Langmuir 16 (2000) 1969–1979.

[24] R. Aveyard, B.P. Binks, J.H. Clint, P.D.I. Fletcher, T.S. Horozov, B. Neumann, V.N. Paunov, et al., Phys. Rev. Lett. 88 (2002) 246102.
[25] T.S. Horozov, R. Aveyard, J.H. Clint, B.P. Binks, Langmuir 19 (2003) 2822–2829.
[26] E.J. Stancik, M. Kouhkan, G.G. Fuller, Langmuir 20 (2004) 90–94.
[27] R. Reynaert, P. Moldenaers, J. Vermant, Langmuir 22 (2006) 4936–4945.
[28] M.E. Leunissen, J. Zwanikken, R. van Roij, P.M. Chaikin, A. van Blaaderen, Phys. Chem. Chem. Phys. 9 (2007) 6405–6414.
[29] L. Isa, K. Kumar, M. Müller, J. Grolig, M. Textor, E. Reimhult, ACS Nano 4 (2010) 5665–5670.
[30] M.A. Ray, L. Jia, Adv. Mater. 19 (2007) 2020–2022.
[31] M.A. Ray, N. Shewmon, S. Bhawalkar, L. Jia, Y. Yang, E.S. Daniels, Langmuir 25 (2009) 7265–7270.
[32] Y. Zhao, J. Wang, G. Mao, Opt. Lett. 30 (2005) 1885–1887.
[33] W.-L. Min, P. Jiang, B. Jiang, Nanotechnology 19 (2008) 475604.
[34] D.G. Stavenga, S. Foletti, G. Palasantzas, K. Arikawa, Proc. Roy. Soc., B 273 (2006) 661–667.
[35] A. Büttner, U.D. Zeitner, Opt. Eng. 41 (2002) 2393–2401.
[36] H. Urey, K.D. Powell, Appl. Opt. 44 (2005) 4930–4936.
[37] Y. Sun, S.R. Forrest, J. Appl. Phys. 100 (2006) 073106.
[38] M. Pitkonen, J. Math. Phys. 47 (2006) 102901.
[39] M. Pitkonen, J. Phys. D: Appl. Phys. 40 (2007) 1483–1488.
[40] J. Jung, T.G. Pedersen, J. Appl. Phys. 112 (2012) 064312.
[41] V.N. Paunov, Colloid Polym. Sci. 281 (2003) 701–707.
[42] D. Frydel, S. Dietrich, Phys. Rev. Lett. 99 (2007) 118302.
[43] A. Domínguez, D. Frydel, M. Oettel, Phys. Rev., E 77 (2008) 020401 (R).
[44] A. Shrestha, K. Bohinc, S. May, Langmuir 28 (2012) 14301–14307.
[45] K.D. Danov, P.A. Kralchevsky, J. Colloid Interface Sci. – Part 2 405 (2013) 269–277.
[46] L.D. Landau, E.M. Lifshitz, Electrodynamics of Continuous Media, Course of Theoretical Physics, vol. 8, Pergamon Press, Oxford, 1960.
[47] K.D. Danov, P.A. Kralchevsky, K.P. Ananthapadmanabhan, A. Lips, Langmuir 22 (2006) 106–115.
[48] K.D. Danov, P.A. Kralchevsky, M.P. Boneva, Langmuir 20 (2004) 6139–6151.
[49] G.A. Korn, T.M. Korn, Mathematical Handbook, McGraw-Hill, New York, 1968.
[50] G. Arfken, Mathematical Methods for Physicists, Academic Press, Orlando, FL, 1970.
[51] P. Moon, D.E. Spencer, Field Theory Handbook, Including Coordinate Systems, Differential Equations, and Their Solutions, Springer-Verlag, New York, 1988.
[52] N.N. Lebedev, I.P. Skalskaya, Y.S. Uflyand, Problems of Mathematical Physics, Prentice Hall, London, 1965.
[53] F.G. Mehler, Math. Ann. 18 (1881) 161–194.
[54] V.A. Fock, Dokl. Akad. Nauk. SSSR 39 (1943) 253–256.
[55] I.N. Sneddon, The Use of Integral Transforms, McGraw Hill, New York, 1972.
[56] V.A. Ditkin, A.P. Prudnikov, Integral Transforms and Operational Calculus, Pergamon Press, Oxford, 1965.
[57] Yu.A. Brychkov, A.P. Prudnikov, Integral Transforms of Generalized Functions, CRC Press, Boca Raton, FL, 1989.
[58] S.B. Yakubovich, Index Transforms, World Scientific, Singapore, 1996.
[59] N.N. Lebedev, Special Functions and Their Applications, Prentice Hall, London, 1965.
[60] M. Abramowitz, I.A. Stegun, Handbook of Mathematical Functions, Dover, New York, 1965.
[61] U. Diebold, Surf. Sci. Rep. 48 (2003) 53–229.
[62] J.Y. Kim, H.S. Jung, J.H. No, J.-R. Kim, K.-S. Hong, J. Electroceram. 16 (2006) 447–451.
[63] B.H. Park, L.S. Li, B.J. Gibbons, J.Y. Huang, Q.X. Jia, Appl. Phys. Lett. 79 (2001) 2797–2799.
[64] K.E. Atkinson, A Survey of Numerical Methods for the Solution of Fredholm Integral Equations of the Second Kind, SIAM, Philadelphia, 1976.
[65] T.B. Jones, Electromechanics of Particles, Cambridge University Press, Cambridge, UK, 1995.
[66] J. Happel, H. Brenner, Low Reynolds Number Hydrodynamics, Kluwer, Boston, 1983.
[67] J.D. Jackson, Classical Electrodynamics, Wiley, New York, 1962.